



Modeling ship-induced waves in shallow water systems: The Venice experiment

D. Bellafiore^{a,*}, L. Zaggia^a, R. Broglia^b, C. Ferrarin^a, F. Barbariol^a, S. Zaghi^b, G. Lorenzetti^a, G. Manfè^a, F. De Pascalis^a, A. Benetazzo^a

^a National Research Council – Institute of Marine Sciences (CNR-ISMAR), Castello 2737/F, 30122, Venice, Italy

^b National Research Council – Marine Technology Research Institute (CNR-INSEAN), Via di Vallerano 139, 00128, Rome, Italy

ARTICLE INFO

Keywords:

Ship waves
CFD
Hydrodynamic model
Tidal flats
Venice lagoon

ABSTRACT

As the size of vessels progressively increases to compete in the global trade, the impact evaluation of navigation in waterways and shallow coastal ecosystems become more important. Therefore, suitable tools to investigate processes are required to support a sustainable management of ship traffic. This work tests a new methodology, based on a numerical model chain, that reproduces the hydrodynamic field close to the ship hull and the ship-induced wave propagation in the surrounding shallow areas. The model chain includes an unstructured hydrodynamic model forced by the near-field estimation of a computational fluid dynamics simulation. The modeling system has been applied to a major navigation channel and surrounding tidal flats in the Venice Lagoon (Italy). Field observations and a theoretical framework were used to characterize the ship waves and to validate the modeling system. Results show that the deeper the initial depression, the larger the dissipation over the tidal flat. In these conditions smaller vessels sailing at higher speed produce smaller waves with low amplitudes compared to larger ships traveling at lower speed. We considered vessels moving at different speeds providing useful information to evaluate impacts and to define criteria for decision support systems for a sustainable management of navigation.

1. Introduction

Shipping is undoubtedly the most efficient way of transporting goods worldwide. However, there are mounting concerns about the impacts of the global traffic on the marine environment both off-shore and on-shore (Zheng et al., 2016). Besides pollution and underwater noise, ship traffic in coastal areas can represent one of the major inputs of energy, in form of disturbance of the hydrodynamic field, which can become a dominant forcing for the morphodynamics of sheltered areas (Soomere, 2005). Moreover, waterways are conveniently located in transitional systems, like estuaries and lagoons, providing a safe access to ports and serving as hubs for inland cities and their industrial and commercial districts. Navigable channels in transitional areas are often the combined result of the anthropic modifications and natural adaptation of the existing morphology to the stress of traffic and they frequently require dredging interventions (Dai et al., 2013; Rosati et al., 2011). The progressive increase in vessel size (Rodrigue, 2013) is a threat for such complex and delicate environments, as large ships moving in channels confined by

tidal flats and marshlands (or simply wetlands) can considerably affect the local morphodynamics (Rapaglia et al., 2011, 2015). These issues are of fundamental importance to define criteria for the sustainable management of the ecosystem and minimize the impacts of navigation.

Critical aspects of monitoring and modeling ship waves in shallow water coastal systems are linked with the intrinsic complexity of the process and the variety of morphological features, like natural and artificial channels, tidal flats and salt marshes. When a vessel is moving in a confined channel the wave pattern produced is the result of the interaction between the hydrodynamic field in the proximity of the hull and the geometry of the channel and its margins. When those are constituted by shallow-water areas, three main factors affect the variation of water level: the speed of the ship, the geometry of the hull and the channel cross-section (Sorensen, 1997). The flow field close to the hull is characterized by a pressure increase at the bow and the stern of the hull, whereas the sides experience a rather flat low-pressure region. In the navigation channel, the hydrodynamics is characterized by backward return currents, parallel and opposite to the ship course, a lateral water

* Corresponding author.

E-mail address: debora.bellafiore@ismar.cnr.it (D. Bellafiore).

level depression, here called *depression wave* according to Rapaglia et al. (2011), Rodin et al. (2015) and Parnell et al. (2015), and a front wave with positive peaks at bow and stern (Fig. 1). These perturbations represent the so called primary waves. The depression wave follows the ship during its transit along the waterway and has a major component of propagation perpendicularly to the channel main axis. The perturbation approaches the channel sides interacting with the morphology (shoaling) and affects the adjacent tidal flats, determining large sediment resuspension (Gelinas et al., 2013) and morphological changes.

The far-field waves in deep water can be classified as transverse and divergent waves (Fig. 1a). Divergent waves, as free surface inertial waves, originate at the bow and stern, or wherever the ship hull does not show a continuous surface. They propagate, in shallow waters, with an angle from the ship longitudinal axis depending on the ship speed and the water depth in the channel. These waves can combine and produce interferences, with visible peaks. Their amplitude increases with the ship speed and can, locally, deepen the depression wave (primary waves) (PIANC, 1987). For an advancing ship in straight course at constant speed the resulting wave system translates with the ship itself; the included half-angle of the wave pattern is called the Kelvin angle. For a ship advancing in deep water, this angle is fixed and it is equal to $19^\circ 28'$. For a ship advancing in finite depth sea, the Kelvin angle depends on the water depth and the ship speed.

The depth based Froude Number $Fr_h = \frac{V}{\sqrt{gH}}$, where V is the ship speed, g is the gravitational acceleration and H is the water depth (Newman, 1977), can help in distinguishing the different waves propagating from the hull. In shallow channels, like the considered one, the limited navigation speed leads to $Fr_h < 1$. In these conditions the most significant perturbation is connected to the lateral depression waves, while Kelvin waves, usually generated in deep waters, are negligible (Rapaglia et al., 2011). These asymmetric, non-linear V-shaped depression waves propagate on the shallows (Rodin et al., 2015; Parnell et al., 2015).

As far as the modeling is concerned, previous studies address the investigation of ship hydrodynamics from different perspectives and with different aims. Most of the works are focused on the near-field analysis

(i.e. a region around the vessels of the order of one ship length). Applications considering vessels operating in open sea (as for example Visonneau et al., 2016; Carrica et al., 2016; Broglia et al., 2015; Dubbioso et al., 2017 and Hirdaris et al., 2016), interacting with the surrounding background field (e.g. Mousaviraad et al., 2015; Volpi et al., 2016; Carrica et al., 2008; Shibata et al., 2012), and advancing in confined channels (e.g. Rodin et al., 2015; Eloat and Vantorre, 2011; Dam et al., 2008; Fleit et al., 2016; Torsvik et al., 2009) can be mentioned. Both Experimental Fluid Dynamics (EFD) tests and Computational Fluid Dynamics (CFD) models are commonly used. For an overview of the state of the art on this topic, the interested reader can refer to the latest workshops on marine hydrodynamics and related topics (Salvatore et al., 2015; Larsson et al., 2013; Simonsen et al., 2014). These studies are mainly focused on local, small scale interaction between the hull and the surrounding water and rarely does the investigation involve far-field hydrodynamics. The main advantage of these models is the high resolution and the capability to reproduce small scale and turbulent processes close to the hull as well as wave pattern, providing a useful indication for ship maneuverability, sea keeping and, in general, naval hydrodynamics related problems. Navigation in confined water (either shallow or restricted waterways) and hydrodynamic interactions due to the passage of multiple ships are also interesting research topics. Different numerical approaches are commonly used, ranging from the Boussinesq 2D models (e.g., Nascimento et al., 2011; Dam et al., 2008) to 3D models (e.g., Yuan et al., 2016; Yao and Dong, 2016) and CFD based tools (e.g., Mousaviraad et al., 2016a), as well as combined EFD studies and CFD implementations (e.g., Eloat and Vantorre, 2011; Fleit et al., 2016; Mousaviraad et al., 2016b).

However, due to the high computational resources required, CFD tools cannot be deemed as the most suitable and efficient approach for the investigation of the propagation of the ship generated waves in the far field. Rather, the use of simplified models has to be considered. The existing literature provides several examples of these models, which consider the channel borders investigating the effects of the ship passage on the surrounding shallow areas, generally adopting idealized and synthetically produced characteristic wave crest (e.g., Torsvik et al., 2009; Dam et al., 2008; Rodrigues et al., 2015). Modeling applications

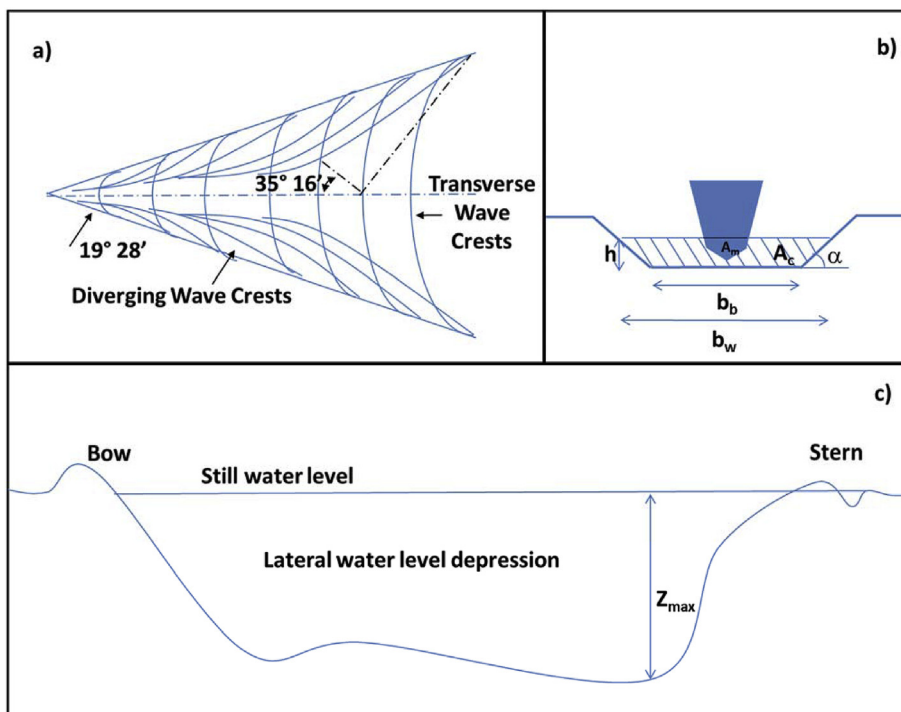


Fig. 1. a) Ship Wave pattern around a moving vessel in deep water (Newman, 1977); b) cross sectional scheme of a navigable channel, with h still water level, A_m wetted area of ship at mid length, A_c wetted area of cross channel section, b_w width of the channel at the surface, b_b width of the channel at the bottom; c) depression wave on a longitudinal section parallel to the main ship axis. The maximum value of the depression wave is hereinafter called Z_{max} . b) and c) schemes are reproduced from (PIANC, 1987).

that studied the propagation of the wave through linear, weakly non-linear or highly non-linear wave theories can be mentioned. Some implementations have recently been performed along a channel section, giving a 1D description of processes (Rodin et al., 2015; Parnell et al., 2015). Therefore, the contribution on the 2D field of different areas of the ship was not considered, not reproducing the background field interactions and approximating the vertical effects of bottom structures. These assumptions could lead to small inconsistencies in comparison with measured data, like time shifts, due to oblique wave interferences. Therefore, by examining the existing literature, a double need arises, to properly reproduce the wave pattern around the hull, specifically the depression wave in its 2D pattern, and to evaluate its propagation outside the channel borders.

This work presents a multi-model tool suitable for simulating ship-induced waves in shallow water systems. The proposed approach considers a high fidelity unsteady Reynolds averaged Navier Stokes Equations model, to accurately describe the flow field inside the channel in the proximity of the vessel, coupled with a finite element hydrodynamic model that reproduces the depression wave propagation in the surrounding shallow water area. The model chain has been applied to the Venice Lagoon and validated against observations acquired in its major waterway and the surrounding tidal flats.

2. Methods - the modeling chain

The numerical model chain used to investigate the hydrodynamic effects determined by the passage of ships in a channel surrounded by tidal flats is composed of a CFD solver (Xnavis) that provides steady state velocity and water level fields in a limited area around the ship hull within the channel and a 3D hydrodynamic finite element model (SHY-FEM) forced by the CFD field along a moving trajectory.

2.1. Xnavis model

The hydrodynamic field that originates around the ship hull advancing straight ahead in a rectilinear channel is computed by the numerical solution of the unsteady Reynolds averaged Navier-Stokes equations, which can be written in integral form as

$$\oint_{S(V)} \mathbf{U} \cdot \mathbf{n} \, dS = 0, \tag{1}$$

$$\frac{\partial}{\partial t} \int_V \mathbf{U} \, dV + \oint_{S(V)} (F_C - F_D) \cdot \mathbf{n} \, dS = 0,$$

where V is the control volume, $S(V)$ its boundary and \mathbf{n} the vector normal to $S(V)$ directed outside the volume. The equations are written in an inertial reference system and are made non dimensional through a reference velocity (the free stream velocity U_0), a reference length (the ship length Lpp) and the water density $\rho = 1026.021 \text{ kg/m}^3$. In the following, results will be discussed in the dimensional form. F_C and F_D represent the non-viscous (advection and pressure contribution) and viscous fluxes, respectively.

$$F_C = p\mathbf{I} + \mathbf{UU}, \tag{2}$$

$$F_D = \left(\frac{1}{Re} + \nu_t \right) (\nabla \mathbf{U} + \nabla \mathbf{U}^T),$$

where p is a new variable related to the pressure P and the acceleration of gravity g (parallel to the vertical axis z) by $p = P + z/Fr^2$, $Fr = U_0 / (g Lpp)^{1/2}$ being the Froude number. $Re = U_0 Lpp / \nu$ is the Reynolds number, ν is the kinematic viscosity ($\nu = 1.189 \cdot 10^{-6} \text{ m}^2/\text{s}$), ν_t is the non-dimensional turbulent viscosity that can be computed by means of several turbulence models implemented in the solver.

Mathematically the system of equation (1) must be completed by appropriate conditions at physical and computational boundaries. On solid walls, the velocity is set to zero (whereas no condition on the

pressure is required). At the inflow boundary, velocity is set to the undisturbed flow value and the pressure is extrapolated from inside. On the contrary, the pressure is set to zero at the downstream boundary, whereas velocity is extrapolated from inner points. To ensure negligible effects on the solution in the region of interest, the inflow and outflow sections are placed far enough. The initial conditions are specified for the velocity.

The numerical solution of the system of equation (1) is computed by the Xnavis code, which is a general-purpose, second order, finite volume, multi-block, unsteady Reynolds averaged Navier-Stokes Equations (uRaNSE) based solver, developed at CNR-INSEAN (National Research Council – Marine Technology Research Institute). A brief description of this numerical tool is given here, the interested reader can refer to the work of Di Mascio et al. (2006), Di Mascio et al. (2007) and Di Mascio et al. (2009).

A numerical approximation for the solution of equation (2) is obtained by partitioning the fluid domain D into N_l structured blocks D^l , each subdivided into $N_x N_y N_z$ disjoint hexahedrons. In the numerical scheme adopted here, the blocks are not necessarily disjoint, but can be partially overlapped. Conservation laws are then applied to each finite volume:

$$\sum_{s=1}^6 \int_{S_s} \mathbf{U} \cdot \mathbf{n} \, dS = 0$$

$$\frac{\partial}{\partial t} \int_{V_{ijk}} \mathbf{U} \, dV + \sum_{s=1}^6 \int_{S_s} (F_C - F_D) \cdot \mathbf{n} \, dS = 0$$

where S_s is the s -th face of the finite volume V_{ijk} , \mathbf{n} is the outward normal and the fluxes are decomposed into a convective part F_C and a diffusive term F_D , as defined in equation (2).

The computation of the convective fluxes and the surface integral of the velocity in the continuity equation can be done by several approximation schemes available in the code, ranging from the first order Godunov scheme, the second order Total Variation Diminishing (TVD) scheme, the third order Essentially Non Oscillatory (ENO) scheme, the third order Weighted ENO (WENO) scheme and the classical fourth order centered scheme (for more details see Di Mascio et al., 2009). Viscous fluxes are discretized by means of the classical finite volumes second order formulation. The free surface effects are simulated through a fully non-linear level-set single phase methodology (Di Mascio et al., 2007).

In order to have a fully implicit scheme and to obtain a divergence free velocity field, a dual (or pseudo) time-derivative is introduced in the discrete system of equations and the solution is iterated to steady state with respect to the pseudo time. The full multi-grid approach and the implicit approximate factorization technique with local time stepping are used to speed up convergence of the internal iteration. The full multi-grid approach is also exploited to assess grid sensitivity: the Richardson's extrapolation technique is used to evaluate numerical uncertainty (Roache, 1997) by the comparison of the solution on each grid-refinement level.

The numerical mesh employed is based on “chimera” grid technique. In this approach, the possibility to let the grids overlap is achieved through a modification of both the boundary conditions and internal point treatment for those zones where overlapping appears: dynamic overlapping grids method allows for easy and accurate handling of complex geometries and multiple bodies in relative motion. Chimera technique requires to locate regions in other blocks from where an approximation of the solution can be extracted, namely it requires to find “donor” cells. Once the donor is identified, a convex set of eight donor cell centers is searched, and a tri-linear interpolation is used to transfer the solution from one block to the one under analysis. If an overlapped cell is found, the cell is marked as a “hole” only if the donor cell is “smaller” (more refined) than the one under analysis. Differently from standard chimera approaches, however, the cell marked as holes are not removed from the computation; instead, the interpolated solution is enforced on the marked cell point by adding a forcing term to the Navier-

Stokes equations, in a “body-force” fashion (for more details see Di Mascio et al., 2006).

High performance computing capabilities are achieved by an efficient shared and distributed memory parallelization (Broglia et al., 2014).

The code has been widely applied for several naval hydrodynamics related problems, for example, maneuverability of surface vessels and submarines, naval propellers and hydrodynamics of multihull vessels (Broglia et al., 2015; Dubbioso et al., 2017; Muscari et al., 2013; Zaghi et al., 2011).

2.2. Shyfem model

The steady state hydrodynamic fields produced by CFD modeling define the shape and characteristics of the ship induced wave. To properly reproduce the propagation of the depression wave through the channel and the tidal flats, a new version of the finite element hydrodynamic model SHYFEM (Umgiesser et al., 2004; Bellafiore and Umgiesser, 2010) was developed.

The model was applied to many transitional environments and coastal systems (Bellafiore and Umgiesser, 2010; Umgiesser et al., 2014; De Pascalis et al., 2011; Ferrarin et al., 2008, 2010; Ghezzi et al., 2010). The model solves shallow water equations, vertically integrated over each layer. Velocities are computed in the center of each element, whereas the water level is computed on the grid nodes. Vertically the model can describe the layers through Z or sigma layers. Horizontal velocities are computed in the center of each layer while the stress and the vertical velocity are computed at the interface between layers.

The horizontal viscosity is parameterized by means of the Smagorinsky formulation (Smagorinsky, 1963; Blumberg and Mellor, 1987), while the vertical viscosity is computed through a k-ε turbulence closure module, an adaptation of the GOTM (General Ocean Turbulence Model) one, described in Burchard and Petersen (1999).

The model adopts a semi-implicit scheme for the temporal discretization. Horizontal diffusion and baroclinic pressure gradients in the momentum equations are treated explicitly. The Coriolis force and the barotropic pressure gradient in the momentum equations and the divergence term in the continuity equation are treated semi-implicitly. The vertical stresses and the bottom friction are computed implicitly, to ensure stability. The spatial discretization follows the Galerkin method, a variation of the classical formulation adopted for finite elements, to avoid numerical damping and to assure mass conservation (Umgiesser et al., 2004).

2.3. Model coupling

We developed a new algorithm, specifically for this implementation, to impose to SHYFEM the hydrodynamic forcing provided by Xnavis (in terms of water levels, computed from provided surface pressure, and 3D velocity). At each time step, output fields from Xnavis are geo-localized in a progressive point of the given ship trajectory within the domain. As it is sketched in Fig. 2, the water levels are interpolated and fixed in an elliptical area, with minor (across channel) and major (along channel) axes smaller than the CFD matrix dimension and centered on the ship mid-point. This specific sub area is, therefore, treated as a boundary area where to force the system with water levels. In the transient area between the described ellipse and the major ellipse inscribed in the CFD matrix, water level values are nudged (relaxation time = time step). This choice allows keeping the original water level pattern fixed in the area close to the ship hull, permitting a progressive relaxation to the SHYFEM shallow water equations solution at the borders of the CFD matrix area. Accordingly, to ensure the correct provision of CFD matrix forcing, stability and the mass conservation in SHYFEM, the 3D velocity field is directly imposed in the whole area covered by the cylinder with basis equal to the major ellipse inscribed in the CFD matrix.

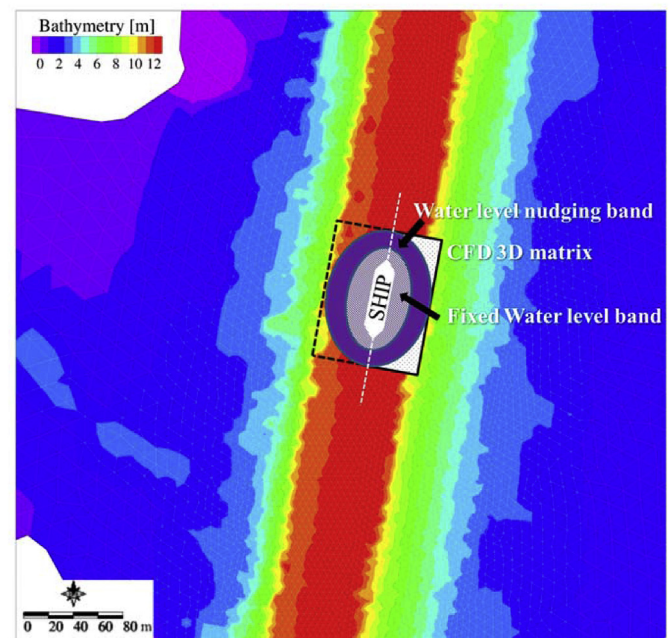


Fig. 2. Sketch of the numerical strategy used to force SHYFEM with 3D outputs of Xnavis along a ship trajectory within a confined channel. The 3D hydrodynamic field (imposed within the dashed square) is mirrored with respect to the ship longitudinal axis. The light purple ellipse bounds the region with water levels in SHYFEM imposed from Xnavis, while, the purple band shows the region where water levels are nudged. The 3D velocities are imposed over the whole purple ellipse. A Finite element grid, with bathymetry of a navigable channel and the nearby tidal flat is shown. (For interpretation of the references to colour in this figure legend, the reader is referred to the Web version of this article.)

3. The Venice experiment

Scientific literature describes several natural and artificial environments that experience an increasing impact due to navigation, like the Elbe Estuary (Silinski et al., 2015), the Kiel Canal (Uliczka and Kondziella, 2016), the Hudson Bay (Zheng et al., 2016), the Mississippi River System (Sorensen, 1997) and many more. The Venice Lagoon and its major waterway, the Malamocco-Marghera Industrial Channel (hereinafter MM channel) represent a paramount example of highly anthropized transitional environments (Sarretta et al., 2010). Therefore, a joint effort, based on two field campaigns, the former investigating the passage of cruise ships, the latter typical commercial ships, and modeling, was performed on the MM channel. Regardless of the peculiar characteristics of this study site, there are substantial analogies with processes and impacts observed in other locations worldwide.

3.1. Study site description

The Venice Lagoon (50 km long, 10 km wide), one of the largest Mediterranean transitional environment, was heavily modified in the last century. In the early 1900, just after the stabilization of the three inlets with jetties, an industrial district (the *Porto Marghera Industrial Zone*) was built at the western border of its central basin. Initially routed across the historic center of the city, commercial ship traffic was successively redirected in the MM channel which was created on purpose in the late '60s to connect the industrial port to the sea, through the Malamocco Inlet (Fig. 3).

The channel has a straight branch 200 m wide and 17 m deep along the east-west direction that connects the inlet to the inner border of the lagoon. It then narrows, along the south-north direction to a 120 m wide, 12 m deep channel that reaches the port facilities. The channel bed is

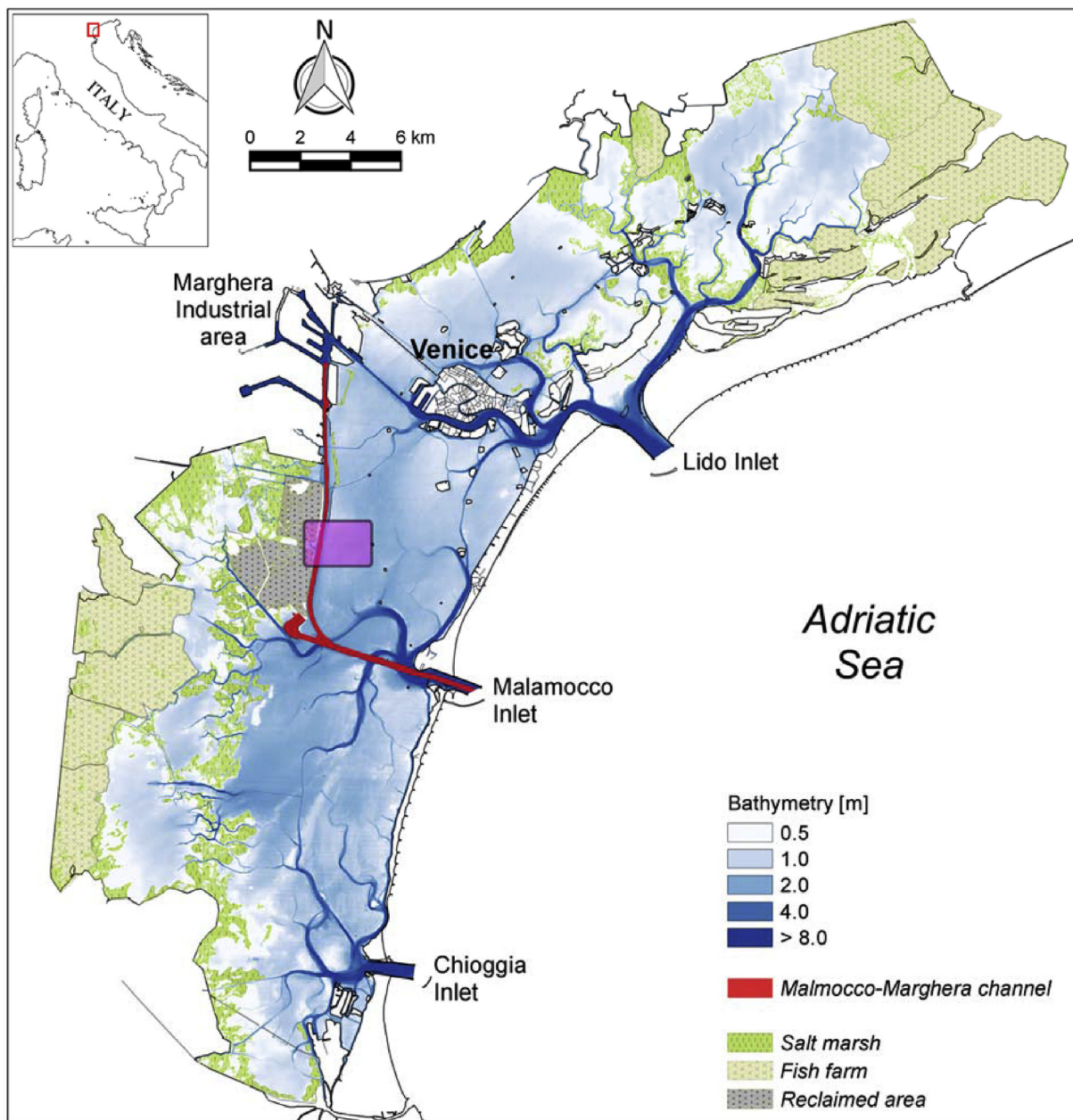


Fig. 3. Bathymetric map of the Venice Lagoon. The purple box indicates the observation study site. (For interpretation of the references to colour in this figure legend, the reader is referred to the Web version of this article.)

100 m and 60 m wide for the two segments respectively and its cross section is trapezoidal on its entire path.

After the excavation of the channel the proximal tidal flats of the central lagoon underwent a progressive generalized erosion (Molinarioli et al., 2009; Sarretta et al., 2010; D'Alpaos, 2010). A recent monitoring of sediment exchanges through time evidenced that material eroded from the central lagoon is not completely flushed away from the lagoon (Defendi et al., 2010) but seems to be mainly deposited in the channels. This trend would determine a general and progressive reduction of morphological feature diversity and loss of habitats in these specific areas (Sarretta et al., 2010; Zaggia et al., 2017). In fact, the port traffic progressively increased, in terms of number of passengers and of number and dimension of cargos, exposing such a morphodynamically active and peculiar transitional environment to additional stresses.

3.2. Field experiments

Ad hoc experimental activities were carried out to investigate ship induced currents and ship wave propagation over the tidal flats in the Venice Lagoon. Two field surveys were conducted:

- on 18th–19th of July 2015, when large cruise ships reached the passenger terminal, located in the historical center of Venice passing through the MM channel;
- on 29th–31st of March 2016, when additional instruments were deployed on the tidal flat bordering the MM channel. Commercial ships were monitored during this survey.

The field activity of the 18–19th of July 2015 was conducted on a portion of the MM channel, 12 m deep and 150 m large, bordered at west

by an area that was reclaimed in the '60 for the expansion of the nearby industrial district of Porto Marghera and by an extended tidal flat to the east. On this side of the channel the mudflat is protected by a breakwater structure located at a distance of about 100 m from the channel (Fig. 4). An electromagnetic current meter (InterOcean Systems S4), recording at a frequency of 2 Hz, was deployed near bottom at 30 m east from the channel main axis (station S2, Fig. 4), providing current velocity and direction, pressure (then converted in corresponding water level values) and turbidity data. A Multi-parametric probe (IDRONAUT OCEAN SEVEN 304 CTD-T), equipped with pressure sensors working at 8 Hz, was deployed at the nearby tidal flat at about 100 m from the channel edge (station B2, Fig. 4).

The first field campaign was performed in spring tide conditions, with maximum vertical water level excursion of 90 cm. All ship passages were in temporal correspondence of the minimum value of tide (low tide).

The second field activity, on the 29th–31st of March 2016, was planned for the investigation on the tidal flat. The instrumental setup was designed to give an accurate indication on the ship wave propagation, even at large distance from the channel (up to 1650 m, Fig. 4).

Each station of the mudflat (B2-B8, Fig. 4) was equipped with a pressure sensor with data logger (RBR - Richard Brancker Recherche - Instruments, Solo) working at a sampling frequency of 16 Hz. At stations B2 and B4 two electromagnetic current meters (InterOcean Systems S4) were deployed, sampling at frequencies of 2 Hz and 5 Hz, respectively. The relatively high sampling frequency was chosen to allow a fair description of the wave features over the innermost part of the tidal flat, where the shape of the wave undergoes a strong modification of its front that introduces short-period oscillations. Moreover, the 2 Hz frequency of the current meter in B2 is considered suitable for the description of the typical depression waves observed in the area (Rapaglia et al., 2011).

Fig. 4 shows also the cross sectional bathymetric profile acquired during the second field campaign. Ship passages were determined from the website <https://www.marinetraffic.com>. The provided information was on the ship passage time and speed, while no data on ship tracks were available.

3.3. Model chain application

The physical process that is studied is strongly influenced by the relative dimensions of the ship and the geometry of the channel. Thus,

given a channel geometry, the principal parameters are the block coefficient and the draft. The block coefficient is defined as the ratio between the displaced volume (∇) and the value of the product of the length, the width and the draught of the ship $C_B = \nabla / (L_{pp} \times B_{WL} \times T)$.

Complete information about the shape of cruise ships in the Venice Lagoon was not available. Therefore, to study a more realistic scenario, the CFD simulations were conducted stretching the dimensions of a basic ship shape, a Japanese bulk carrier (JBC, mono-propeller, $C_B = 0.85$) for which the geometry was available. The re-shaping procedure has been pursued keeping fixed the value of the block coefficient to 0.7, typical of the cruise ships entering the Venice Lagoon (as deduced from Rapaglia et al., 2011 and Rapaglia et al., 2015), which is considered as the main parameter affecting the physical model. The limit of the adopted procedure is that bow and stern's phase could be somehow different from a typical cruise ship. Anyway this aspect provides larger effect on the generated wave pattern, close to the ship, and minor effects on the far field pattern. Moreover, although bulk carriers can sometimes have large drafts up to 10 m, the typical draft of cargo ships is comparable to cruise ships' drafts monitored in the Venice Lagoon (around 8.5 m). Two re-shapings were considered and the principal dimensions of the two simulated ships are reported in Table 1: SHIP1 was just stretched, partially re-shaped and linearly rescaled in order to reduce the JBC block coefficient to 0.7. From that, keeping C_B , SHIP2 was re-shaped to meet the dimensions of Cruise ship Costa Deliziosa as much as possible, for validation purposes. The two re-shapings represent the typologies of cruise ships sailing through the Venice Lagoon, allowed inferences to be made on the impact of different draughts on the wave propagation.

Simulations with Xnavis were conducted in a rectilinear channel with a constant cross section corresponding to the geometry of the MM channel, close to the investigated area (Fig. 5), where the experimental measurements were performed. In the simulations, the channel was

Table 1
Principal dimensions of the ships simulated.

Ship particulars	SHIP1	SHIP2
Length L_{pp} (m)	300.0	294.0
Width B_{WL} (m)	32.0	32.3
Draught T (m)	8.7	8.0
Displacement ∇ (m ³)	120×10^3	108×10^3
Block coefficient C_B (-)	0.7	0.7

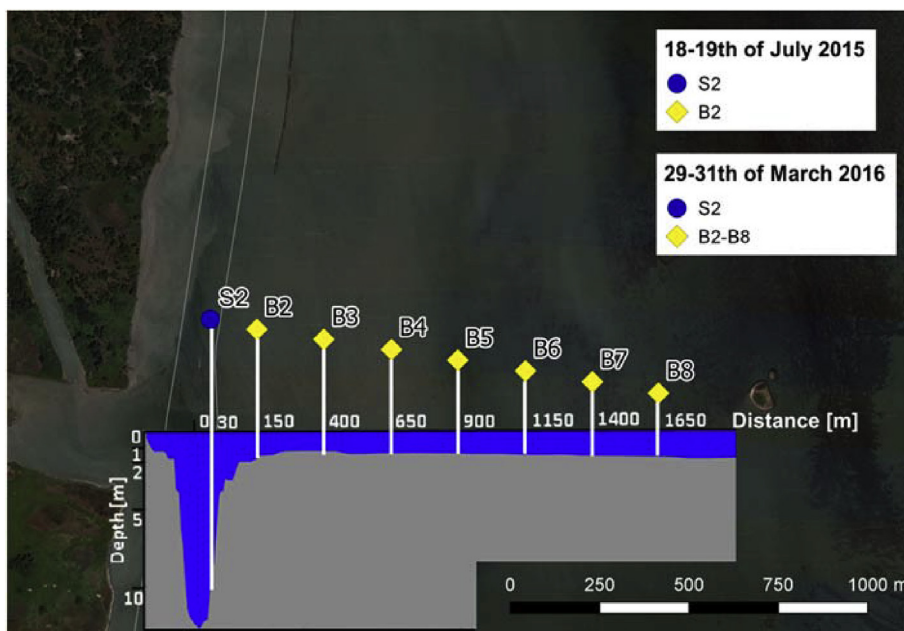


Fig. 4. Location of in situ instruments used for the measurements during the field campaigns in the MM channel and in the nearby tidal flat. The 18th–19th of July 2015, blue dot represents the S4 instrument, located in S2 station at the bottom of the border of the channel, and the yellow diamond in B2 represents the pressure probe on the tidal flat; the 29th–31st of March 2016, yellow diamonds represent pressure sensors in B2-B8 from the channel to the inner tidal flat, with an average spacing of 250 m. In B2 and B4 also the S4 instruments were deployed. The corresponding bathymetric profile is superimposed at bottom. (For interpretation of the references to colour in this figure legend, the reader is referred to the Web version of this article.)

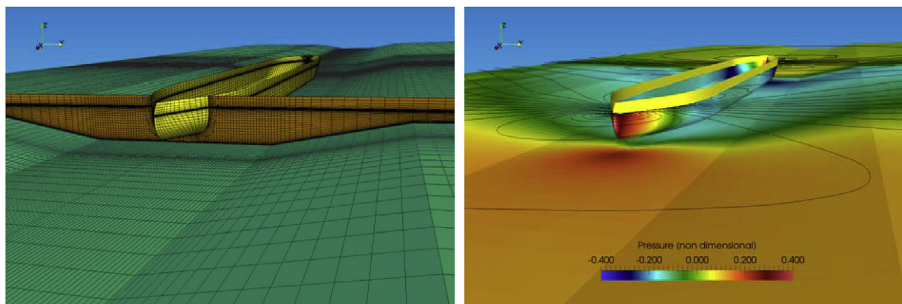


Fig. 5. CFD computations. Left, volume mesh, in the picture the grid on the surface of the hull, on the bottom and on a cross section are reported; for clearness purposes every fourth points are shown. Right, pressure on the hull surface and on the bottom; black lines represent free surface levels. The hull is from the re-shaped bulk carrier SHIP-1.

considered left/right symmetric, with the longitudinal axis of the ship corresponding to the channel axis. Therefore, the numerical domain reproduced is one half of the channel.

The discretization of the fluid-dynamical field around the ship is obtained exploiting the overlapping grids capabilities of the solver (Fig. 5, left). In particular two zones were considered, one in the proximity of the ship hull and the other one covering the entire channel. For the region close to the hull, several structured, overlapped and adjacent blocks, body fitted on the surface of the hull, are used. The specific resolution is driven by geometrical consideration (higher resolution in region of higher curvature) and by fluid-dynamics considerations (higher resolution where larger gradients of the field variables are expected). In particular the cells are only slightly clustered toward solid wall surfaces, the simulation being inviscid. In fact, viscous forces have negligible effects on the wave pattern, the domain of interest being small if compared with the major wavelength generating from the ship, thus no relevant viscous dispersion happens. The grid covers an area up to 660 m upstream and downstream the ship and 200 m laterally. To accurately consider all the effects from the boundaries and the variation of the cross section of the channel, a very fine discretization has been made, ranging from 0.1 m to a few meters. This accounts for about 22 millions of finite volumes used for the discretization of the channel and a total of 24.5 millions of volume for the whole CFD mesh.

We did not account for the effects produced by propellers, as it is reasonable to consider them negligible for the propagation of the depression wave. The air/water interface was treated with a single level-set technique, which guarantees a fully non-linear treatment of the free surface, including its deformation. To accurately describe the wave system, a very refined grid resolution in the free surface region has been considered. Indeed, the numerical tests performed with a fixed surface and linearized boundary conditions have shown less accuracy in the results and an underestimation of the ship wave amplitude. The flow field is resolved in the ship reference system and velocity is considered stationary. In Fig. 5 (right) the pressure field on the hull surface and on the bottom wall is reported as an example of CFD solution. High pressure regions are seen close to the bow and the stern of the ship (i.e. at the stagnation points), whereas a rather large flat low pressure region is predicted along the side of the vessel. It is interesting to note the deep depression that develops close to the stern region: this is clearly a consequence of the acceleration of the flow beneath of the vessel due to the Bernoulli effects. The strong depression region is typical during the navigation in very shallow water and the consequent squat can cause ship grounding.

Table 2

List of numerical simulations with corresponding ship speed and Froude number (Fr).

Numerical experiment	Ship speed (kn)	Fr
SHIP1-1	8.60	0.415
SHIP1-2	7.70	0.372
SHIP2-1	8.60	0.415

The 3D hydrodynamic outputs of Xnavis, interpolated on a Cartesian block centered around the hull, having resolution of 0.7 m, 0.7 m, 0.4 m in the x, y, z directions, are used as forcing for the SHYFEM simulations. The numerical mesh of SHYFEM describes with 26037 nodes and 51638 triangular elements (resolution ranging from 3 m to 40 m, see example of the mesh in Fig. 2) a portion of the Venice Lagoon adjacent to the MM channel (Fig. 3, purple square). The computational domain was chosen to represent the area covered by the field measurements. The bathymetry is based on the dataset collected by *Magistrato alle Acque di Venezia* (MAV) in 2002 (and merged with following surveys) and on data measured by ISMAR-CNR in 2014 in the main channels of the Venice Lagoon. Comparing the cross sectional bathymetric profile acquired during the second field campaign with the one obtained from this dataset some discrepancies arise. The current tidal flats are slightly deeper, about +30 cm, and the channel slightly shallower (−30 cm) compared to the depth resulting from measurements of MAV in 2002.

The SHYFEM simulations run imposing 12 vertical sigma layers, to reach at most a maximum thickness of 1 m in the MM channel and higher vertical resolution in shallower areas of the domain. The Coriolis effects are not considered due to the limited area of the domain. TVD (Total Variation Diminishing) schemes are used for horizontal and vertical advection.

The numerical experiments were performed evaluating a first ship (SHIP1 in Table 1) sailing at two different speeds (8.6 kn and 7.7 kn) and a second ship (SHIP 2 in Table 1) sailing at 8.6 kn. The three experiments were planned to validate the setup, investigating the effect of a different ship geometry, particularly the effect of draught, at a given speed (SHIP1-1 and SHIP2-1, Table 2), and to state the variation in the wave signal just due to reduced velocities (SHIP1-1 and SHIP1-2, Table 2).

For the specific channel simulated, the mean water level was set to −23 cm to account for the tidal condition at the time of the observations.

4. Results and discussion

4.1. Depression wave characterization and model validation

The waves created by cruise ship passages were monitored in the investigated section during the field measurement of July 18–19th 2015 (stations S2, in the channel, and B2, in the tidal flats). The sea surface elevation measured during the passage of the ship *Costa Deliziosa* (the 19th of July 2015, at 4:28 UTC) in the MM channel directed to the Cruise Terminal is used to validate the model chain results. Fig. 6 shows the comparison between the depression waves and currents taken during the passage of the ship *Costa Deliziosa* and the model-chain results, in correspondence of stations S2, in the channel, and B2, in the nearby tidal flat.

As it was seen in previous works (Rapaglia et al., 2011; Parnell et al., 2015), the depression wave developed in the channel is characterized by a deep trough, with an almost symmetrical shape around the minimum level. High frequency oscillations are registered before the maximum depression (Z_{\max} in Fig. 1) and after the passage of the ship. The former is probably due to local effects induced by the hull, while the latter results

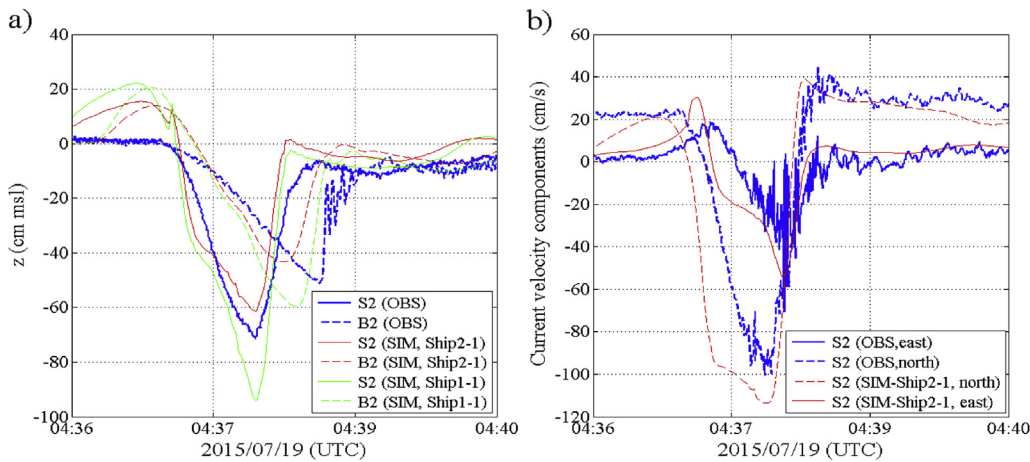


Fig. 6. Time series of observed (OBS) and simulated (SIM) water level (a) and current speed (b) at the position of instruments S2 and B2. The water level for SHIP1-1 and SHIP2-1 simulations is shown, while east and north components of the current velocities are plotted only for SHIP2-1 simulation.

from the interference of the primary depression wave with the secondary waves during the restoration of the pressure field in still conditions.

Once the depression wave reaches the tidal flat (position B2), the value of Z_{max} is attenuated by the interaction with the bottom and the wave shape changes to the well documented asymmetric V-shape (Fig. 6, Parnell et al., 2015).

The water level decreased at S2 of about 70 cm with respect to the still condition, while on the tidal flat Z_{max} was approximately 50 cm. The instrument placed on the channel bottom recorded no clear evidence of an increase of the sea level at the beginning of the disturbance.

The SHIP1-1 simulation shows a maximum depression of -94 cm, which overestimates the observation (-71 cm). The difference could partially be explained by a larger immersed surface of the hull, corresponding to a draught of 8.7 m, instead of the draught of the real case (8.0 m).

To verify this hypothesis and better understand the origin of the discrepancy, we also considered the results from SHIP2-1 simulation, which considers a smaller draught than SHIP1-1 simulation, i.e. comparable with the one of the measured ship. The results of this second run are in better agreement with the observations in S2, even if underestimating the measured value of about 10 cm. A similar discrepancy is found at station B2. The computed waves for both simulated ships differ from measurements in reproducing the positive peak (about +20 cm), registered both in the channel and in the tidal flat before the depression. Analyzing the steady state field produced by Xnavis, we found that the model seems to enhance the peak due to the pressure effect at the bow and at the stern. This discrepancy could probably be due to the numerical assumptions (non-viscous flow, absence of the propeller). Additionally, the simulated geometry, being a re-scaling of a bulk carrier type, is different from the real ship and this aspect can influence the wave pattern, producing lower local attenuation of the signal. However, due to the local nature of these processes, characterized by wave lengths lower than the principal wave signal, their influence is negligible on the wave propagation over the tidal flat.

The ship wave reproduced by the modeling chain reaches the tidal flat (position B2) 14.8 s earlier than the measurements. Probably the approximations applied for the SHYFEM set up, as the hydrostatic approximation that inhibits the vertical acceleration and the shallow water approximation of equations, can be responsible for the observed time shift. However, the time shift results smaller than the value obtained with other numerical approaches, as, for example, the one proposed by Parnell et al. (2015), where the signal simulated by the 1D non-linear model is slower and shows a delay of 40 s from measurements.

Modeled bottom velocities were also assessed against measurements. During the ship passage the measured current speed on the MM channel bottom was predominantly directed along the channel main axis (negative values in Fig. 6) with a southward component of 120 cm s^{-1} three

times larger than the westward component. The measured signal in S2 shows a tidal current directed northward before the passage of the ship along the channel main axis. During the ship passage, first there is an increase in the current toward east, followed by an opposite current. The maximum value of current is higher than 1 m s^{-1} , directed to south-west. We note (not shown here) that the disturbance induced by the ship lasted for about 15 min after the passage, on both the channel and the tidal flat. All simulations show a similar pattern of currents generated by the ship passage, both in direction and speed. The simulations do not consider the tide as forcing and this can justify the small discrepancies with the observations.

To interpret the noted discrepancies, at least in the depression wave amplitude, between measured and modeled results, a theoretical model evaluating the energy balance of the process was applied. Following the approach proposed by Schijf (PIANC, 1987), it is possible to define a maximum ship speed suitable for navigation in restricted channels (V_L) by solving the following implicit equation:

$$\frac{V_L}{\sqrt{gh}} = \left(\frac{2}{3}\right)^{1.5} \left(1 - \frac{A_m}{A_c} + \frac{V_L^2}{2gh}\right)^{1.5} \quad (3)$$

where $h' = \frac{A_c}{b_w}$, A_m is the wetted area of ship at mid length, A_c is the wetted area of cross channel section, b_w is the width of the channel at the surface and b_b is the width of the channel at the bottom (Fig. 1). The mean water level depression D_h can be computed solving the system:

$$D_h = \frac{V_s^2}{2g} \left[\alpha_1 \left(\frac{A_c}{A_w}\right)^2 - 1 \right] \quad (4)$$

$$A_w = b_b(h - D_h) + m(h - D_h)^2 - A_m$$

where V_s is the ship speed, A_w is the wetted cross sectional area at the ship passage, h is the still water level, m is the slope of the channel bank, $\alpha_1 = 1.4 - 0.4 \frac{V_s}{V_L}$.

The theoretical model was assessed against the results of measurements performed during the 18–19th of July 2015 campaign, which have blockage ratio A_m/A_c (i.e., the ratio of the immersed ship area A_m to channel cross sectional area A_c , Fig. 1) ranging from 0.13 to 0.16, and variable speed from 7.4 kn to 9.0 kn. The full list of considered ships, with their geometric characteristics, speed and the measured Z_{max} in S2 and B2 is reported in Appendix.

The monitored ships generally navigate at higher speed while leaving the lagoon, thus the corresponding Z_{max} are larger, compared to ships with same blockage ratios (i.e. MSC POESIA, MSC MAGNIFICA and MSC MUSICA, see appendix). Primarily, it should be mentioned that the channel cross-section has a different shape before and after the monitoring stations and consequently ships move through portions of channel

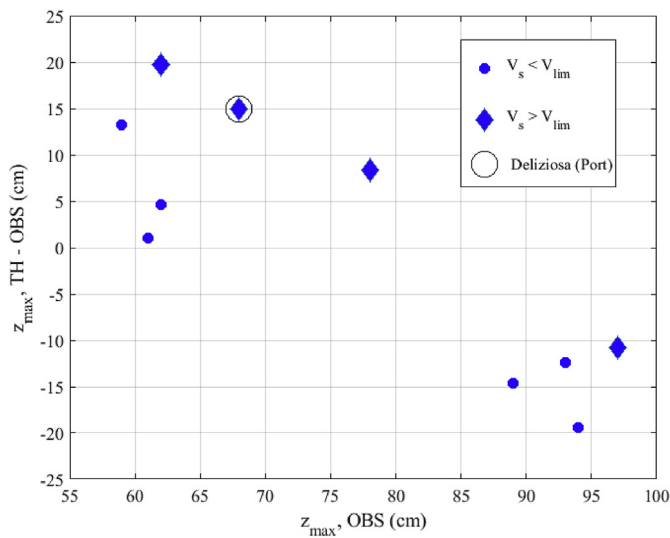


Fig. 7. Mean absolute difference between the measured Z_{max} (OBS) and the theoretical estimation D_h (TH) obtained following the Schijf formulation. Diamonds represent ship speed exceeding the limit velocity $V_s > V_{lim}$, for which $V_s = 0.95V_{lim}$ has been imposed in the computation, following the applicability limits declared in PIANC (1987). The black circle represents the test ship used for validation that travelled along the channel the morning of the 19th of July 2015.

that have different confinement (blockage ratio). Additionally, the route of the ships does not always follow the central axis of the channel, therefore observed effects could differ from those expected. Despite the lack of information from the available measurements, these aspects were analyzed in literature and studies can be mentioned that address it (Wang and Zou, 2014, Lataire and Vantorre, 2008 and references therein): entering a part of the channel with higher confinement (lock) increases the velocity of return flow, with sudden changes in the hydrodynamics in the portion of channel where there is the highest change in the section (Meng et al., 2015). Moreover, the presence of banks gives rise to interaction processes with the ship and if the ship is sailing closest to one of the channel sides (eccentricity), this would lead to asymmetries also in the lateral wave generation: the lateral depression would be more pronounced and there could occur an attractive force that move the ship close to the bank (Lataire and Vantorre, 2008). Therefore we should take into account the possible effects of bank effects (shape, distance, slope) and sailing trajectory (possible eccentricity) on the amplitude of the depression wave.

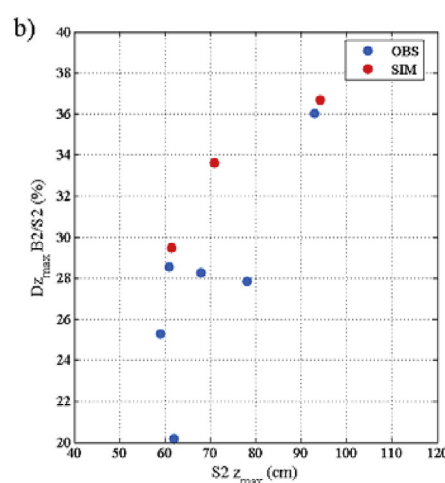
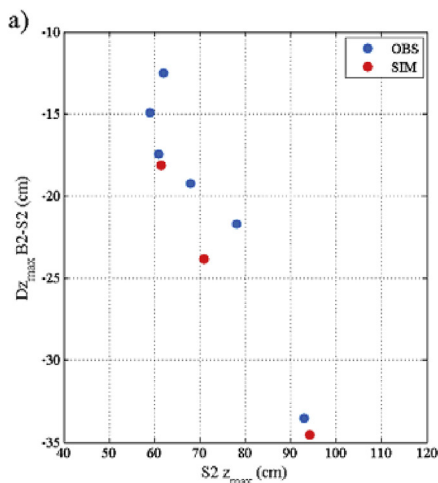


Fig. 8. Left Attenuation of Z_{max} between S2 (center) and the tidal flat (B2) close to the MM channel, compared to the value in S2. Blue dots show the observations, and the red dots represent modeled values computed with SHYFEM. a) absolute values; b) percentage values. (For interpretation of the references to colour in this figure legend, the reader is referred to the Web version of this article.)

Following the Schijf formulation, measured and theoretically expected depression wave amplitude are shown in Fig. 7. The maximum depression measured in S2, cannot be properly defined as Z_{max} because the monitoring station does not correspond to the center of the channel and ship eccentricity is not known. Therefore, the comparison is made between the measured maximum depression values and theoretical D_h .

It has to be noted that some ships travelled with a speed exceeding the critical ship speed and, therefore, did not properly fulfill the assumptions of the approximate energy approach. Nevertheless, the comparison shows agreement between measured and theoretical results, with a mean absolute difference of about 12 cm, which we assume acceptable within the adopted approximations. Indeed, the channel section used for the computation has been approximated with a trapezoidal shape and the ship passages, entering and exiting the channel, were similarly treated, even if the channel section changes before and after the monitored zone. Moreover, there is no information about the eccentricity of the ship trajectory respect to the longitudinal axis of the channel (a similar analysis using eccentricity of 15 m would increase the mean absolute difference of 3 cm). All these aspects can justify the discrepancies between the theoretical computation and the measurements.

However, the theoretical model allows quantifying the expected Z_{max} induced by the ships, confirming the correlation with ship speed and geometry (blockage ratio). By computing the mean depression wave with the Schijf model for the Cruise ship Costa Deliziosa passage, taking into account the modeled geometries and speeds of SHIP1 and SHIP2, a Z_{max} decrease of 15 cm due to the smaller area of the immersed section of the latter ship is expected that could, finally, explain the discrepancy seen in Fig. 6.

The dissipation of potential energy between the channel center (S2) and the tidal flat (B2) is evaluated in Fig. 8 as the difference between Z_{max} at the two locations for all the cruise ships that were measured in the 18–19th of July campaign. In general, the larger the disturbance in the channel (and thus the current speed induced by the drawdown), the larger the dissipation along the course between the two stations. Indeed, the maximum difference of about 35 cm is associated with the shallower depression in the channel, resulting in more than 90 cm. In percentage, the differences, respect to the amplitude in the center of the channel, range between 20 and 36%.

Looking at Fig. 8 it can be noted that the model results are in reasonable agreement with measurements, probably matching the dissipation processes that would justify the observed increase in the attenuation rate respect to the wave amplitude in the channel. However, there is a small overestimation (5%) in modeled attenuation rates which could be ascribed to differences in the bathymetry imposed to the model. The excess of modeled dissipation can be due to the above mentioned small discrepancy between the used and the real bathymetry, with a

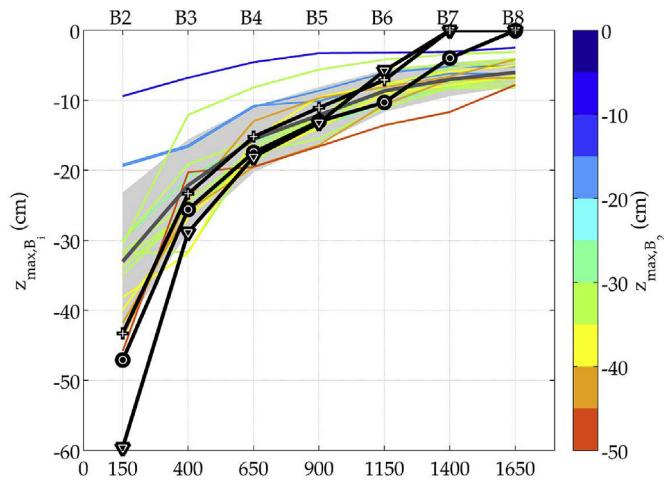


Fig. 9. Z_{\max} values in the tidal flat adjacent to the MM channel (B2-B8). Coloured lines represent values measured at stations B2-B8 during the 16 ships passages (29th–31st of March 2016 campaign) with colours representing the initial depression wave in B2. The average of the 16 ship passages and the confidence interval (average plus or minus the standard deviation) are represented by the gray solid line and the gray shaded region, respectively. The black lines represent the modeled values (crosses – SHIP1-2 simulation, speed 7.7 kn; triangles – SHIP1-1 simulation, speed 8.6 kn; circles – SHIP2-1 simulation, speed 8.6 kn). (For interpretation of the references to colour in this figure legend, the reader is referred to the Web version of this article.)

shallower tidal flat close to the channel compared with the actual situation, enhancing the effects of bottom stress.

4.2. Assessment of shipwave propagation on the tidal flats

Depression waves created by the traffic of commercial vessels (container ships, bulk carriers and tankers) were acquired during the field measurements of the 29th–31st of March 2016. We monitored 40 ships navigating in the channel, but only a sample of 16 vessels was used for the analysis after a quality check on the recorded data. The observed and modeled depressions over the tidal flat stations are shown in Fig. 9.

The seven stations shown (B2-B8, Fig. 4) are located in a tidal flat zone that progressively varies from a depth of 1.9 (B2) to 0.9 m (B5-B6) and then to 1.5 m (B7-B8). Hence, we expected most of the dissipation occurring within approximately the first kilometer from the channel axis. The depression waves have a mean value of –33 cm in B2 where, however, values have a wide range (36 cm) that depends on the different geometry and speed of the monitored ships. The depression wave is progressively attenuated toward the center of the tidal flat, passing from a mean value of –9 cm (with a range of 8 cm) at station B6 to a mean value of –6 cm at station B8 (with a range of 6 cm). This suggests that, as expected, the most dissipative region of the tidal flat is between B2 and B6, which corresponds to the zone with the largest gradient in water depth. The deepest depressions in B2 are the ones that are damped the most in the propagation over this part of the tidal flat.

All the described features are evident in Fig. 10 where the wave attenuation over the tidal flat stations is defined as a percentage of the value in station B2. Considering the average trend, station B6 registers an attenuation of about 73%, while in station B8 the attenuation is about 80% of the initial B2 value, as an average. This confirms that stations B2 and B6, where depth is decreasing progressively, bound the area characterized by the maximum attenuation rate. In B8, the minimum and maximum attenuations correspond to 68% and 91% (Fig. 10) showing that a considerable range of attenuations occurs.

Fig. 10 also shows how, over the tidal flats, the modeled depression waves are generally larger than those measured in B2, in particular SHIP1-1 simulation at 8.6 kn speed. In fact, this run considers ship

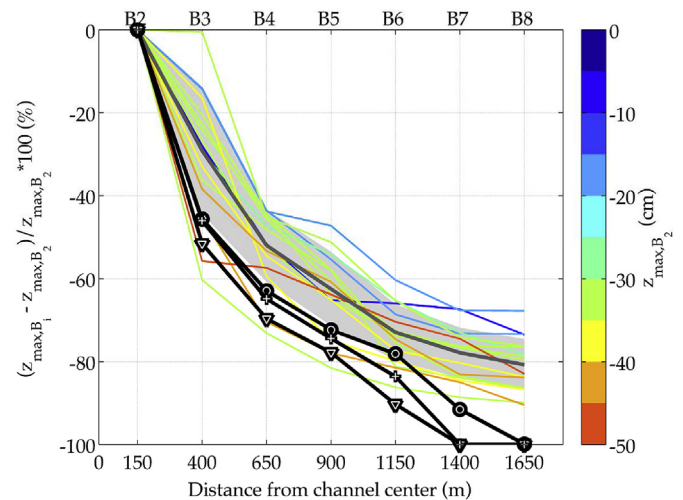


Fig. 10. Dissipation of Z_{\max} (as % of Z_{\max} in B2) in the tidal flat adjacent to the MM channel. Coloured lines represent values measured at stations B2-B8 during the 16 ships passages (29th–31st of March 2016 campaign) with colours representing the initial Z_{\max} in B2. The average of the 16 ship passages and the confidence interval (average plus or minus the standard deviation) are represented by the gray solid line and the gray shaded region, respectively. The black lines represent the modeled values (crosses – SHIP1-2 simulation, speed 7.7 kn; triangles – SHIP1-1 simulation, speed 8.6 kn; circles SHIP2-1 simulation, speed 8.6 kn). (For interpretation of the references to colour in this figure legend, the reader is referred to the Web version of this article.)

parameters that lead to a higher blockage ratio and ship speed compared to the ones in the measured dataset. In any case the model dissipation reproduces fairly well the observed trend, within station B2 and B5, where depth is progressively decreasing. Model outputs show that in the most distant stations from the channel center the signal is completely attenuated.

The modeling chain allows inferring about some specific dependency relations, not always so easy to verify from measurements because of the variety of concurrent factors, as the response of the system to varying speeds with a fixed geometry or to different ships traveling at the same speed. In Fig. 11 the attenuation rate for the two simulations SHIP1-1 and SHIP1-2, is shown. It is evident how the increase in ship speed enhances the amplitude of the depression and the attenuation rate. The deepest depression in the center of the channel, the largest its interaction with the tidal flat dynamics by bottom stress effects and dissipation with consequences on the morphology of the channel-tidal flat system.

On the other hand, considering SHIP1-1 and SHIP2-1 simulations, it is evident that the ship with the smaller draft propagated a smaller depression wave (–61 cm vs. –95 cm).

Another important aspect that is evidenced by Fig. 11 is that ships with smaller draught but higher speeds (SHIP2-1 simulation, 8.6 kn) produced a slightly smaller depression compared to bigger ships traveling at lower speeds (SHIP1-2 simulation, 7.7 kn).

In order to complete the analysis of the three simulation results, we evaluate the distributions of maximum depression and normalized maximum depression referred to the residual water level (Fig. 12). What can be deduced is that, for all simulations, for the test-velocities the area characterized by maximum depressions deeper than 10 cm reaches the tidal flat, identifying a possible area of influence due to the ship passage within station B4. This aspect is in good agreement with the results of measurements. Comparing SHIP 1-1 and SHIP 1-2, the increase in speed does not change significantly the area of influence but the maximum depressions are larger, particularly in the tidal flat close to the channel (normalized maximum depression 0.4 vs 0.5). If we consider the passage of different ships at the same velocity (SHIP 1-1 and SHIP 2-1), an enlargement of the area of influence for the ship with the bigger draft is found. Also the absolute maximum depressions are bigger. Therefore it

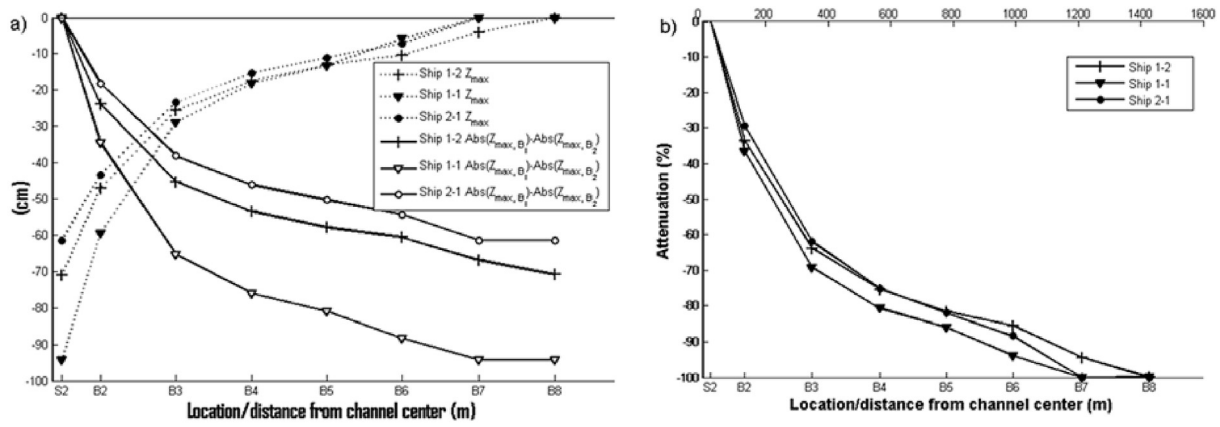


Fig. 11. Attenuation of Z_{max} (m). a) maximum depression (dashed) and absolute difference with S2 (line). b) percentage of the maximum depression registered in the center of the channel still present in the locations along the section of the MM channel, for SHIP1-2 simulation, speed 7.7 kn (cross), SHIP1-1 simulation, speed 8.6 kn (triangle) and SHIP2-1 simulation, speed 8.6 kn (circle).

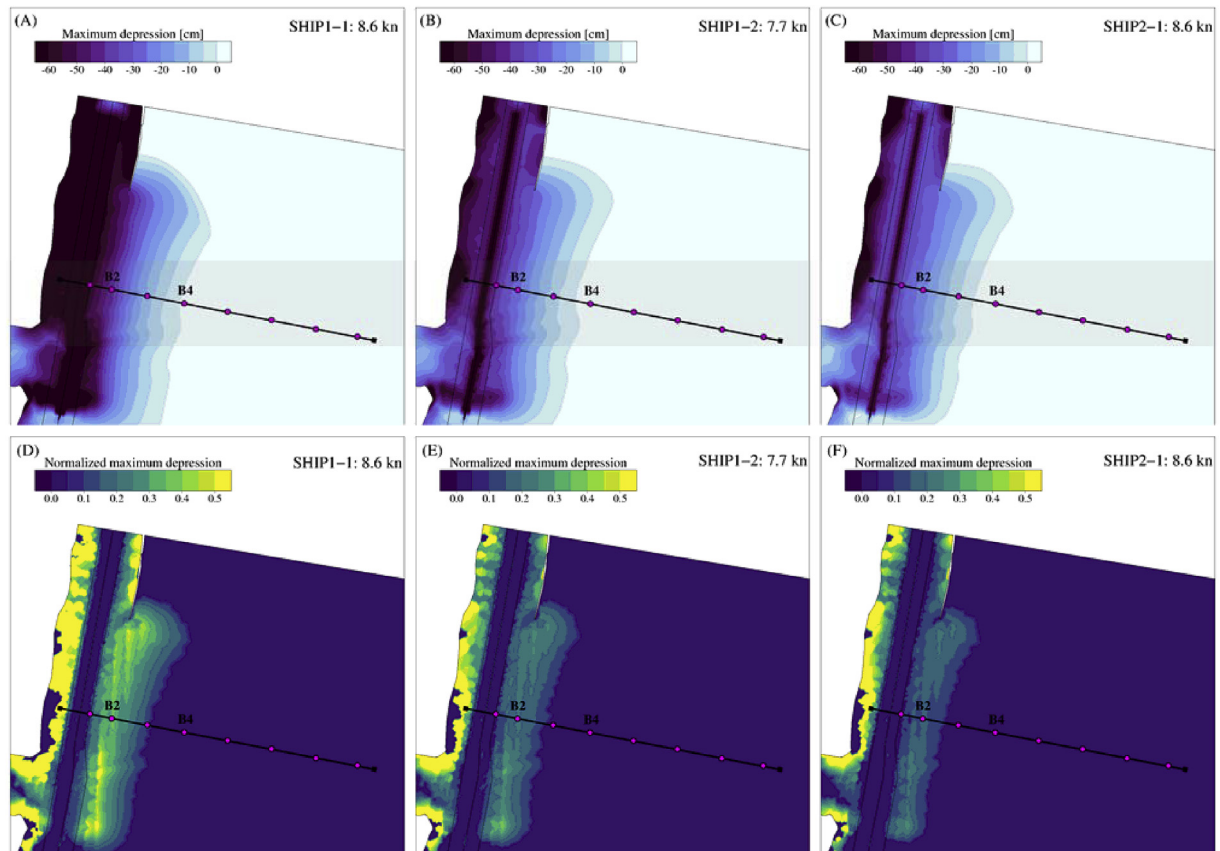


Fig. 12. Maps of maximum depression (panels a, b and c) and normalized maximum depression referred to the residual water level (panels d, e and f) for SHIP 1-1, SHIP 1-2 and SHIP 2-1 simulations in the MM channel.

can be concluded that the passage of a ship with bigger dimensions, deeper draft but lower speed influences a larger area of the tidal flat than a ship with smaller dimensions and higher speed.

5. Conclusions and perspectives

Ship wakes formation and propagation in confined channels is a topic tackled by several scientists and engineers dealing with theoretical issues and impacts on coastal environments. This research work tests a numerical methodology that keeps the required degree of physical complexity and provides outcomes of primary importance for

environmental protection and easily applicable for management. The tool allows for the investigation of the hydrodynamics in a waterway around the ship hull (through a CFD solver) and propagation of the pressure perturbation in the surrounding shallow areas (through a shallow water unstructured model).

The novelty of the proposed approach is the combined implementation of different numerical tools able to provide an accurate description of both the local and far-field processes. This approach could eventually include local effects related to the viscosity and the presence of propellers, considering highly detailed ship geometries.

Although some approximations were introduced in the proposed

approach, the numerical model chain has been successfully validated against observations of water levels and currents collected in the Venice Lagoon.

The modeling tool complements the information from the field activities and previous works, investigating the “what if” option connected with different ship sizes or navigation speed. These are two factors influencing the shape and propagation of lateral wave level depression, among a number of other ones, which can be better analyzed when data for comparison are available, such as the channel geometry (width, depth, bank slope) and the real ship track eccentricity. The first test evidenced how the ship geometry plays a fundamental role in producing ship wakes that can be still visible at a large distance from the navigation channel over the tidal flat. For the considered ship speed range, still higher than the existing speed limits for navigation in the channel, but consistent with the velocities measured during ship transits in our field experiments, smaller and faster ships seem to have less impact on the tidal flat than bigger vessels navigating at relatively lower speeds. Further sensitivity analyses can provide a full range of options, within the

maximum-minimum speed limits that guarantee ship maneuverability, which could easily be considered in specific Decision Support Systems (DSS).

This analysis suggests that the developed tools could be further refined to introduce other hydrodynamic drivers, like atmospheric forcing and tides, needed to match the complexity of the real case. Moreover, the numerical models could be also used to investigate the effect of ship waves on sediment resuspension and morphodynamics of complex coastal systems such as lagoons or estuaries.

Acknowledgements

This work was partially funded by the Port Authority of Venice and carried out through a research service (“STATO AMBIENTALE DELLA LAGUNA DI VENEZIA ED ELEMENTI PER LA PIANIFICAZIONE SOSTENIBILE DELLE ATTIVITÀ PORTUALI”) for CORILA (Consorzio per il coordinamento delle ricerche inerenti al sistema lagunare di Venezia).

Appendix

Table 1

Cruise ship passages surveyed during the first field campaign, July 18–19th, 2015: maximum depression Z_{\max} measured by the instrumentation. Ships directed to the Cruise Terminal are identified with the tag *Port*, while the opposite travel direction of ships to the Venice Lagoon Inlets is tagged as *Sea*. The ship characteristics were obtained from the cruise companies websites. Ship speed provided by the website <https://www.marinetraffic.com>.

SHIP NAME	Date and Time (UTC)	Direction	Dimensions: length (m)x width (m)x draft(m)	Speed V_S (kn)	Station B2 Z_{\max} (cm)	Station S2 Z_{\max} (cm)
MSC LIRICA	18/07/2015 04:55	Port	275.9 × 32.0 × 6.8	7.7	52	70
MSC POESIA	18/07/2015 05:26	Port	293.8 × 32.2 × 7.8	7.4	55	68
MSC POESIA	18/07/2015 16:06	Sea	293.8 × 32.2 × 7.8	9	62	86
MSC LIRICA	18/07/2015 17:19	Sea	274.9 × 32 × 6.8	8.4	50	65
COSTA DELIZIOSA	19/07/2015 04:28	Port	294 × 32.3 × 8	8.6	53	75
MSC MAGNIFICA	19/07/2015 05:24	Port	293.8 × 32.2 × 7.8	7.8	70	105
MSC MUSICA	19/07/2015 05:24	Port	293.8 × 32.2 × 7.8	8.3	54	74
MSC MAGNIFICA	19/07/2015 16:22	Sea	293.8 × 32.2 × 7.8	8.7	68	96
COSTA DELIZIOSA	19/07/2015 16:59	Sea	294 × 32.3 × 8	8.3	71	103
MSC MUSICA	19/07/2015 17:11	Sea	293.8 × 32.2 × 7.8	9.2	74	109

References

- Bellafore, D., Umgiesser, G., 2010. Hydrodynamic coastal processes in the North Adriatic investigates with a 3D finite element model. *Ocean Dynam.* 60, 255–273.
- Blumberg, A.F., Mellor, G.L., 1987. A description of a three-dimensional coastal ocean circulation model. In: Heaps, N.S. (Ed.), *Three-dimensional Coastal Ocean Models*. American Geophysical Union, Washington, D.C.
- Brogli, R., Dubbioso, G., Durante, D., Di Mascio, A., 2015. Turning ability analysis of a fully appended twin screw vessel by CFD. Part I: single rudder configuration. *Ocean Eng.* 105, 275–286.
- Brogli, R., Zaghi, S., Muscari, R., Salvatore, F., 2014. Enabling Hydrodynamics Solver for Efficient Parallel Simulations (Bologna, Italy).
- Burchard, H., Petersen, O., 1999. Models of turbulence in the marine environment—a comparative study of two-equation turbulence models. *J. Mar. Syst.* 21, 29–53.
- Carrica, P., Paik, K.J., Hosseini, H.S., Stern, F., 2008. URANS analysis of a broaching event in irregular quartering seas. *J. Mar. Sci. Technol.* 13 (4), 395–407.
- Carrica, P., Kerkvliet, M., Quadvlieg, F., Pontarelli, M., Martin, J., 2016. CFD simulations and experiments of a maneuvering generic submarine and prognosis for simulation of near the surface operation. In: *31st Symposium on Naval Hydrodynamics* (Monterey, California).
- Dai, Z., Liu, J.T., Fu, G., Xie, H., 2013. A thirteen-year record of bathymetric changes in the North Passage, Changjiang (Yangtze) estuary. *Geomorphology* 187, 101–107.
- D'Alpaos, L., 2010. L'evoluzione morfologica della Laguna di Venezia attraverso la lettura di alcune mappe storiche e delle sue carte idrografiche. Venice Municipality, Venice.
- Dam, K.T., Katsutosh, T., Eldina, F., 2008. Investigation of ship waves in a narrow channel. *J. Mar. Sci. Technol.* 13 (3), 223–230.
- De Pascalis, F., Perez-Ruzafa, A., Gilabert, J., Marcos, C., Umgiesser, G., 2011. Climate change response of the Mar Menor coastal lagoon (Spain) using a hydrodynamic finite element model. *Estuar. Coast Shelf Sci.* 114, 118–129.
- Defendi, V., Kovacevic, V., Arena, F., Zaggia, L., 2010. Estimating sediment transport from acoustic measurements in the Venice Lagoon inlets. *Contin. Shelf Res.* 30 (8), 883–893.
- Di Mascio, A., Muscari, R., Brogli, R., 2006. An overlapping grids approach for moving bodies problems. In: *Proceedings of 16th Int. Offshore and Polar Engineering Conference*. San Francisco, California (USA).
- Di Mascio, A., Brogli, R., Muscari, R., 2007. On the application of the single-phase level set method to naval hydrodynamic flows. *Comput. Fluids* 36, 868–886.
- Di Mascio, A., Brogli, R., Muscari, R., 2009. Prediction of hydrodynamic coefficients of ship hulls by high-order Godunov-type methods. *J. Mar. Sci. Tech.* 14, 19–29.
- Dubbioso, G., Brogli, R., Zaghi, S., 2017. CFD analysis of maneuvering characteristics of a submarine model. accepted to *Ocean Eng.* 129, 459–479.
- Eloot, K., Vantorre, M., 2011. Ship behaviour in shallow and confined water: an overview of hydrodynamic effects through EFD. In: *Presented at the RTO-AVT Specialists' Meeting on Assessment of Stability and Control Prediction Methods for NATO Air and Sea Vehicles*.
- Ferrarin, C., Razinkov, A., Gulbinskas, S., Umgiesser, G., Bliudziue, L., 2008. Hydraulic regime based zonation scheme of the Curonian lagoon. *Hydrobiologia* 611 (1), 133–146.
- Ferrarin, C., Umgiesser, G., Bajo, M., De Pascalis, F., Bellafiore, D., Mattassi, G., Scroccaro, I., 2010. Hydraulic zonation of the lagoons of Marano and Grado, Italy, A modelling approach. *Estuar. Coast Shelf Sci.* 87 (4), 561–572.
- Fleit, G., Baranya, S., R  ther, N., Bihs, H., Kramer, T., Jozsa, J., 2016. Investigation of the effects of ship induced waves on the littoral zone with field measurements and CFD modeling. *Water* 8, 300.
- Gelinas, M., Bokuniewicz, H., Rapaglia, J., Lwiza, K.M.M., 2013. Sediment resuspension by ship wakes in the Venice lagoon. *J. Coast Res.* 29, 8–17.
- Ghezzi, M., Guerzoni, S., Cucco, A., Umgiesser, G., 2010. Changes in Venice Lagoon dynamics due to construction of mobile barriers. *Coast. Eng.* 57, 694–708.
- Hirdaris, S.E., Lee, Y., Mortola, G., Incecik, A., Turan, O., Hong, S.Y., Kim, B.W., Kim, K.H., Bennet, S., Miao, S.H., Temarel, P., 2016. The influence of non linearities on the symmetric hydrodynamic response of a 10,000teu containership. *Ocean Eng.* 111, 166–178.
- Larsson, L., Stern, F., Visonneau, M., 2013. *Numerical Ship Hydrodynamics an Assessment of the Gothenburg 2010 Workshop*. Springer.

- Lataire, E., Vantorre, M., 2008. Ship-bank interaction induced by irregular bank geometries. In: 27th Symposium on Naval Hydrodynamics (Seoul, Korea).
- Meng, Q., Wan, D., Wenhua, H., 2015. Numerical Investigation of Influence of Eccentricity on the Hydrodynamics of a Ship Maneuvering into a Lock. ICCM, Auckland, NZ.
- Molinarioli, E., Guerzoni, S., Sarretta, A., Masiol, M., Pistolato, M., 2009. Thirty-year Changes (1970 to 2000) in Bathymetry and Sediment Texture Recorded in the Lagoon of Venice Sub-basins, Italy, vol 258, pp. 115–125.
- Mousaviraad, S.M., Sadat-Hosseini, H., Carrica, P.M., Stern, F., 2016b. Ship–Ship interactions in calm water and waves. Part 2: URANS validation in replenishment and overtaking conditions. *Ocean. Eng.* 111, 627–638.
- Mousaviraad, S.M., Sadat-Hosseini, H., Stern, F., 2016a. Ship–ship interactions in calm water and waves. Part 1: analysis of the experimental data. *Ocean. Eng.* 111, 615–626.
- Mousaviraad, S.M., Wang, Z., Stern, F., 2015. URANS studies of hydrodynamic performance and slamming loads on high-speed planing hulls in calm water and waves for deep and shallow conditions. *Appl. Ocean Res.* 51, 222–240.
- Muscari, R., Di Mascio, A., Verzicco, R., 2013. Modeling of vortex dynamics in the wake of a marine propeller. *Comput. Fluids* 65–79.
- Nascimento, M., Neves, C., Maciel, G., 2011. Waves generated by two or more ships in a channel. *Coast. Eng. Proc.* 1 (32).
- Newman, J.N., 1977. *Marine Hydrodynamics*. MIT Press.
- Parnell, K.E., Soomere, T., Zaggia, L., Rodin, A., Lorenzetti, G., Rapaglia, J., Scarpa, G.M., 2015. Ship-induced solitary riemann waves of depression in Venice lagoon. *Phys. Lett. A* 379, 555–559.
- PIANC, 1987. Permanent International Association of Navigation Congresses, “Guidelines for the Design and Construction of Flexible Revetments Incorporating Geotextiles for Inland Waterways PTC1 Report of WG 4 – 1987.
- Rapaglia, J., Zaggia, L., Parnell, K., Lorenzetti, G., Vafeidis, A.T., 2015. Ship-wake induced sediment remobilization: effects and proposed. *Ocean Coast Manag.* 110, 1–11.
- Rapaglia, J., Zaggia, L., Ricklefs, K., Gelinas, M., Bokuniewicz, H., 2011. Characteristics of ships' depression waves and associated sediment resuspension in Venice Lagoon, Italy. *J. Mar. Syst.* 85, 45–56.
- Roache, J.P., 1997. Quantification of uncertainty in computational fluid dynamics. *Annu. Rev. Fluid Mech.* 29, 123–160.
- Rodin, A., Soomere, T., Parnell, K.E., Zaggia, L., 2015. Numerical simulation of the propagation of ship-induced riemann waves of depression into the Venice lagoon. *Proc. Est. Acad. Sci.* 64 (1), 22–35.
- Rodrigue, J.-P., 2013. *The Geography of Transport Systems*. Routledge, New York.
- Rodrigues, S.R.A., Guedes Soares, C., Santos, J.A., 2015. Propagation of Waves Generated by a Pressure Disturbance Moving in a Channel. Taylor & Francis, London, UK.
- Rosatí, J.D., Sanchez, A., Tate, 2011. The mystery of historical channel shoaling at the Houston-Galveston navigation channel. In: Wang, P., Rosatí, J.D., Roberts, T.M. (Eds.), *Coastal Sediments 2011*. World Scientific, Miami, Florida.
- Salvatore, F., Broglia, R., Muscari, R., 2015. In: Proceedings of VI International Conference on Computational Methods in Marine Engineering (Rome, Italy).
- Sarretta, A., Pillon, S., Molinarioli, E., Guerzoni, S., Fontolan, G., 2010. Sediment budget in the lagoon of Venice, Italy. *Continental Shelf Res.* 30 (8), 934–949.
- Shibata, K., Koshizuka, S., Sakai, M., Tanizawa, K., 2012. Lagrangian simulations of ship-wave interactions in rough seas. *Ocean. Eng.* 42, 13–25.
- Silinski, A., Heuner, M., Schoelynck, J., Puijalón, S., Schröder, U., Fuchs, E., Troch, P., Bouma, T.J., Meire, P., Temmerman, S., 2015. Effects of wind waves versus ship waves on tidal marsh plants: a flume study on different life stages of *Scirpus maritimus*. *PLoS One* 10 (3).
- Simonsen, C.D., Quadvlieg, F., Stern, F., 2014. In: Proceedings of SIMMAN 2014: Workshop on Verification and Validation of Ship Manoeuvring Simulation Methods (Copenhagen, Denmark).
- Smagorinsky, J., 1963. General circulation experiments with the primitive equations. *Mon. Weather Rev.* 91 (3), 99.
- Soomere, T., 2005. Fast ferry traffic as a qualitatively new forcing factor of environmental processes in non-tidal sea areas: a case study in tallinn bay, baltic sea. *Environ. Fluid Mech.* 5, 293–323.
- Sorensen, R.M., 1997. Prediction of Vessel-generated Waves with Reference to Vessels Common to the Upper Mississippi River System. U.S. Army Engineer Waterways Experiment Station, & Upper Mississippi River-Illinois Waterway System Navigation Study, Vicksburg.
- Torsvik, T., Pedersen, G., Dysthe, K., 2009. Waves generated by a pressure disturbance moving in a channel with a variable cross-sectional topography. *J. Waterw. Port, Coast. Ocean Eng.* 120–123.
- Uliczka, K., Kondziella, B., 2016. Ship-induced sediment transport in coastal waterways (SeSt) – VZB. In: Proceedings in 4th MASHCON (Hamburg).
- Umgiesser, G., Melaku Canu, D., Cucco, A., Solidoro, C., 2004. A finite element model for the Venice Lagoon. Development, set up, calibration and validation. *J. Mar. Syst.* 51, 123–145.
- Umgiesser, G., Ferrarin, C., Cucco, A., De Pascalis, F., Bellafiore, D., Ghezzi, M., Bajo, M., 2014. Comparative hydrodynamics of 10 Mediterranean lagoons by means of numerical modeling. *J. Geophys. Res. Oceans* 119 (4), 2212–2226.
- Visonneau, M., Deng, G., Guilmineau, E., Queutey, P., Wackers, J., 2016. Local and global assessment of the flow around the Japan bulk Carrier with and without energy saving devices at model and full scale. In: 31st Symposium on Naval Hydrodynamics (Monterey, California).
- Volpi, S., Diez, M., Sadat-Hosseini, H., Kim, D.H., Stern, F., Thodal, R.S., Grenestedt, J.L., 2016. Full-scale fluid-structure interaction simulation and experimental validation of high-speed planing-hull slamming with composite panels. In: 31st Symposium on Naval Hydrodynamics (Monterey, California).
- Wang, H.-Z., Zou, Z.-J., 2014. Numerical prediction of hydrodynamic forces on a ship passing through a lock. *China Ocean Eng.* 28 (3), 421–432.
- Yao, C.B., Dong, 2016. Numerical study on local steady flow effects on hydrodynamic interaction between two parallel ships advancing in waves. *Eng. Anal. Bound. Elem.* 66, 129–144.
- Yuan, Z.M., Ji, C.Y., Incecik, A., Zhao, W., Day, A., 2016. Theoretical and numerical estimation of ship-to-ship hydrodynamic interaction effects. *Ocean. Eng.* 121, 239–253.
- Zaggia, L., Lorenzetti, G., Manfè, G., Scarpa, G.M., Molinarioli, E., Parnell, K.E., Rapaglia, J.P., Gionta, M., Soomere, T., 2017. Fast shoreline erosion induced by ship wakes in a coastal lagoon: field evidence and remote sensing analysis. *PLoS One* 12 (10) e0187210.
- Zaghi, S., Broglia, R., Di Mascio, A., 2011. Analysis of the interference effects for high-speed catamarans by model tests and numerical simulations. *Ocean. Eng.* 38 (17), 2110–2122.
- Zheng, W., Mo, Z., Shun, C., Sperling, D., 2016. Pollution: three steps to a green shipping industry. *Nature* 530, 275–277.